Archival Report

Biological Psychiatry: CNNI

Quantification of Metabotropic Glutamate Receptor 5 Availability With Both [^{11}C]ABP688 and [^{18}F]FPEB Positron Emission Tomography in the *Sapap3* Knockout Mouse Model for Obsessive-Compulsive–like Behavior

Dorien Glorie, Jeroen Verhaeghe, Alan Miranda, Stef De Lombaerde, Sigrid Stroobants, and Steven Staelens

ABSTRACT

BACKGROUND: This study provides a first direct comparison between positron emission tomography radioligands targeting the allosteric site of the metabotropic glutamate receptor 5 (mGluR5): [^{11}C]ABP688 and [^{18}F]FPEB. A blocking paradigm was set up to substantiate the common binding site of both radioligands. Second, both radioligands were applied in *Sapap3* knockout (KO) mice showing compulsive-like behavior characterized by a lower in vivo mGluR5 availability.

METHODS: First, wild-type mice (n = 7) received four position emission tomography/computed tomography scans: a [^{11}C]ABP688 scan, a [^{18}F]FPEB scan, and two blocking scans using cold FPEB and cold ABP688, respectively. A second experiment compared both radioligands in wild-type (n = 7) and KO (n = 10) mice. The simplified reference tissue model was used to calculate the nondisplaceable binding potential representing the in vivo availability of mGluR5 in the brain.

RESULTS: Using cold FPEB as a blocking compound for [^{11}C]ABP688 micro–positron emission tomography and vice versa, we observed averaged global reductions in mGluR5 availability of circa 98% for [^{11}C]ABP688 and 82%–96% for [^{18}F]FPEB. For KOs, the [^{11}C]ABP688 nondisplaceable binding potential was on average 25% lower compared with wild-type control mice ($p < .0001$–$.001$), while this was about 17% for [^{18}F]FPEB ($p < .05$).

CONCLUSIONS: The current findings substantiate a common binding site and suggest a strong relationship between mGluR5 availability levels measured with both radioligands. In *Sapap3* KO mice, a reduced mGluR5 availability could therefore be demonstrated with both radioligands. With [^{11}C]ABP688, higher significance levels were achieved in more brain regions. These findings suggest [^{11}C]ABP688 as a preferable radiotracer to quantify mGluR5 availability, as exemplified here in a model for compulsive-like behavior.

https://doi.org/10.1016/j.bpsc.2021.11.010

Various neurologic and psychiatric disorders were shown to be associated with a dysfunctional glutamate transmission such as obsessive-compulsive disorder (OCD) (1,2). OCD is a severe psychiatric disorder with a lifetime prevalence of 1%–3% (3) and is characterized by recurrent and persistent thoughts/urges/images (obsessions) and/or by time-consuming repetitive thoughts/actions (compulsions) to neutralize these obsessions (4,5). The first-line pharmacological treatment consists of selective serotonin reuptake inhibitors. Unfortunately, a considerable number of patients remains refractory (6), emphasizing the need for new superior treatment options. In the past 2 decades, the glutamate system has emerged as an important player in the pathophysiology of OCD based on preclinical, genetic, and imaging studies (7–14). There may be a role for the mainly peri- and postsynaptic G protein–coupled metabotropic glutamate receptor 5 (mGluR5), which modulates glutamate neurotransmission and neuronal excitability (15). Both suppression and induction of compulsive-like behavior was possible via the administration of mGluR5 allosteric modulators (16). In addition, multiple promising glutamate modulators were tested (17–19). Although promising, the overall results remain inconclusive. A common conclusion comprises the need for larger study populations, considering symptom dimensions and comorbidities (20).

Different validated positron emission tomography (PET) tracers (21) enable the in vivo visualization of mGluR5 distribution, both in the preclinical and the clinical setting with a high translational potential. Moreover, this highly sensitive, noninvasive imaging modality allows regional and longitudinal quantification of mGluR5 availability in health and disease. This

ISSN: 2451-9022

can provide valuable insights in underlying disease mechanisms and could facilitate the search for novel and superior therapeutics. Currently, there are two commonly used radioligands to image mGluR5 with PET: [^{11}C]ABP688 (22) and [^{18}F]FPEB (23). Both are negative allosteric modulators, and therefore they do not compete with endogenous glutamate for binding at the orthosteric site (1,24). In addition, they seem to target solely cell surface receptors, not internalized receptors (25). Both tracers are characterized by adequate blood-brain barrier penetration, a specific reversible binding to mGluR5, and favorable brain kinetics, in the absence of troublesome metabolites (26,27). In theory, [^{18}F]FPEB offers different advantages. In vitro, it has a higher affinity for mGluR5 (K_D = 0.04 ± 0.02 nM – 0.15 ± 0.11 nM) (28) compared with [^{11}C]ABP688 (K_D = 1.7 ± 0.2 nM) (22) and is thought to have a higher specificity. In addition, the F-18 isotope has a longer half-life, which contributes to a higher cost-effectiveness as a larger number of subjects can be imaged with a single radiotracer production. The short half-life of C-11 requires an on-site cyclotron. However, for F-18, possible defluorination in the skull could hamper quantification. Both radiotracers have already made important contributions to the understanding of the role of this receptor in health and disease (1,2,21). For OCD, one study demonstrated significant correlations between the [^{11}C]ABP688 distribution volume ratio and the Yale-Brown Obsessive Compulsive Scale obsessions subscore within the cortico-striato-thalamocortical circuit (29).

Both [^{11}C]ABP688 and [^{18}F]FPEB can be blocked by the administration of other mGluR5 negative allosteric modulators such as MPEP and MTEP (26,30–32). These findings provide indirect evidence that both tracers bind the same, or close to the same, site of the receptor (33). To date, it remains unclear whether either of these two probes will prove to be preferable. A first step is to further verify their common binding site via the quantification of mGluR5 with both [^{11}C]ABP688 and [^{18}F]FPEB within one animal, followed by a paradigm in which [^{11}C]ABP688 is blocked with unlabeled "cold" FPEB and vice versa (Figure S1). To date, no direct within-subject comparison between both radiotracers has been reported for both humans and animals. A second aim is to verify whether [^{18}F]FPEB, similar to [^{11}C]ABP688, is able to capture a significantly lower mGluR5 availability (34) in the *Sapap3* knockout (KO) mouse model (12). These mice lack the SAP90/PSD-95 associated protein (*Sapap3*), which belongs to the group of scaffolding proteins that link different types of glutamate receptors at the level of the postsynaptic density (35,36). They show excessive pathological grooming, increased anxiety-like behavior, and an imbalanced striatal output and were proposed as a model for OCD (16). Third, taking together the two previous study goals as a common end point, we consider the correlation between the [^{11}C]ABP688 and [^{18}F]FPEB regional nondisplaceable binding potential (BP_{ND}) outcome parameters, which represent receptor availability, for separate animals.

METHODS AND MATERIALS

Mice

Mice were bred inhouse at the University of Antwerp from heterozygous *Sapap3*$^{+/-}$ breeder pairs (kindly obtained from Professor Dr. Feng, Massachusetts Institute of Technology). Genotypes were determined via polymerase chain reaction on mouse ear DNA. Both the animals of experiment 1 (male C57BL/6J: wild-type [WT] n = 7) and experiment 2 (male C57BL/6J: WT n = 7; *Sapap3*$^{-/-}$ KO, n = 10) were kept under the same conditions. They were cohoused in individually ventilated cages under controlled conditions (12 hours normal light/dark cycles, 20–23 °C, and 50%–55% relative humidity) with water and rodent food pellets ad libitum. All animals were scored biweekly for skin lesions, based on the severity. Figure S1 provides an overview of all experimental procedures. All animal procedures were performed in accordance with the European Ethics Committee approval (decree 86/609/CEE). The study protocol was approved by the Animal Experimental Ethical Committee of the University of Antwerp, Antwerp, Belgium.

Tracer Synthesis

Based on a previous description of the radiosynthesis (22), [^{11}C]ABP688-E was prepared as such (34). The injected cold mass was aimed at <5.00 nmol/kg to avoid cold mass effects (37) (Table S1). For the blocking experiment, the mean molar activity (A_m) at the time of injection was 43.19 ± 6.66 MBq/nmol for the test scans and 29.93 ± 3.48 MBq/nmol for the blocking scans. In experiment 2 comparing genotypes, the mean A_m was 59.35 ± 12.22 MBq/nmol for the WT and 53.84 ± 10.63 MBq/nmol for the KO group.

[^{18}F]FPEB was synthesized using 3-chloro-5-([pyridine-2-yl])ethynyl]benzonitrile at high molar activities and radiochemical yield on an automated synthesis module (Comecer). [^{18}F]fluoride, produced by irradiation of [^{18}O]H_2O via ^{18}O(p, n)^{18}F nuclear reaction (cyclotron; Siemens Eclipse), was trapped on a Sep-Pak QMA cartridge (Waters), and eluted into a V-shaped reaction vial with a solution of Kryptofix 222 (12 mM) and K_2CO_3 (6 mM) in MeCN/H_2O (96/4, 1.5 mL). The solvents were azeotropically distilled at 90 °C under a stream of helium. After that, anhydrous acetonitrile (1 mL) was added, and distillation was continued. This process was repeated until a dry white residue was obtained. The reaction vial was heated to 180–190 °C, and the FPEB precursor (5–6 mg), dissolved in 0.5 mL anhydrous dimethyl sulfoxide (DMSO), was added. The resulting mixture was refluxed for 20 minutes, and, after cooling, quenched by addition of sterile water (1.5 mL) and purified using isocratic semipreparative reverse phase high-performance liquid chromatography (Phenomenex Kinetex 5 μm EVO C18 100 Å 10 × 150 mm, λ = 254 nm; mobile phase: NaOAc 0.05 M pH 5.5/EtOH 60/40 vol/vol, 3 mL/min). The collected radioactive product was diluted with 15 mL of sterile water and passed through Sep-Pak Alumina N and Sep-Pak tC18 cartridges assembled together in this order. The cartridges were washed with sterile water (5 mL), and pure [^{18}F]FPEB was released with 96% EtOH (0.5 mL), diluted with sterile saline (5 mL), and filtered in a sterile manner. Radiochemical purity was determined. The total synthesis time, calculated from the end of bombardment and including high-performance liquid chromatography purification, was approximately 70 minutes. Typical irradiation of the target lasted 20 minutes with a beam current of 60 μA. The injected cold mass was aimed at <3.00 nmol/kg to avoid cold mass effects (37)

(Table S1). For the blocking experiment, the mean A_m at the time of injection was 144.8 ± 41.21 for the test scans and 90.02 ± 46.83 MBq/nmol for the blocking scans. In experiment 2 comparing genotypes, the mean A_m was 142.60 ± 53.98 MBq/nmol for the WT and 140.80 ± 64.70 MBq/nmol for the KO group.

Behavioral Evaluation

For experiment 2 (Figure S1), prior to micro-PET (μPET) scanning, each animal was monitored by video recording to assess the grooming behavior. All 30-minute recordings and manual scorings were performed according to a previously described protocol (34).

Cross-sectional [^{11}C]ABP688 and [^{18}F]FPEB Dynamic (Blocking) μPET/Computed Tomography Scans

Both the cohorts from experiments 1 and 2 were subjected to a baseline dynamic μPET/computed tomography (CT) acquisition with both [^{11}C]ABP688 and [^{18}F]FPEB (Figure S1). Mice were anesthetized using isoflurane (IsoFlo) mixed with medical oxygen (induction 5%, maintenance 2%) and placed on a heated blanket (37.5 °C). A catheter (tubing: P10, Instech Solomon; needle: BD Microlance 30G; BD) was placed in the tail vein for later intravenous bolus administration of the tracer. Afterward, the animals were positioned on the heated bed of the scanner. Parallel to the start of the 60-minute dynamic μPET acquisition, a 0.2-mL bolus of the radioligand was administered using an automated syringe pump at a rate of 1 mL/min (model 11 Elite; Harvard Apparatus). Subsequently, a 10-minute 80 kV/500-μA CT scan was acquired for attenuation and scatter correction. Acquisitions (60 + 10 min; frames: 12 × 10 s, 3 × 20 s, 3 × 30 s, 3 × 60 s, 3 × 150 s, and 9 × 300 s) were performed on two Siemens Inveon μPET/CT scanners (Siemens Preclinical Solutions). During scanning procedures, both the respiratory and heart rates were monitored and body temperature was kept at 37.0 °C with a feedback airflow system (Minerve). For the blocking scans, a 0.1-mL intravenous 5% dimethyl sulfoxide in saline bolus containing either unlabeled ABP688 (11.9 mg/mL) or FPEB (0.2 mg/mL) was administered 5 minutes prior to the radiotracer injection. The animal and the scan parameters are represented in Table S1.

Image Processing

μPET images were reconstructed using two-dimensional ordered subset expectation maximization with four iterations and 16 subsets after Fourier rebinning. The images were reconstructed on a 128 × 128 × 159 grid with a voxel size of 0.776 × 0.776 × 0.796 mm. Normalization, dead time correction, random subtraction, CT-based attenuation, and simulated single-scatter corrections, as well as detector response modeling for parallax errors, were applied (38). Reconstructed images were processed in PMOD version 3.6 (PMOD Technologies). For all test images, a static image corresponding to the time-averaged frames of each dynamic acquisition was spatially transformed to a mouse brain [^{11}C]ABP688 or [^{18}F]FPEB PET template (in-house), respectively. This PET template (via CT) already corresponded to a standardized magnetic resonance template space (Waxholm MR) (39) with the corresponding volume of interest (VOI) definitions. The obtained matrix from the aforementioned brain normalization step was applied to transform all dynamic scans to that [^{11}C]ABP688 template space. For all blocking images, the CT of the blocking scan was manually matched to the CT of the test scan of the same animal. This transformation was applied to the dynamic blocking image. The resulting dynamic blocking image was then subjected to an identical image processing pipeline as its corresponding test scan. The regional time-activity curves (TACs) were extracted from the resulting raw nonsmoothed images via the superimposition of the VOI template. For both radioligands, the extracted TACs served as an input for the simplified reference tissue model (40). Based on this method (implemented in PMOD), the regional BP_{ND} was calculated with the cerebellum as an earlier validated reference region (26,27). Based on the spill-in effect of anterior brain structures on the cerebellum and the skull defluorination present with [^{18}F]FPEB, the cerebellar VOI was concentrically reduced. Pixelwise kinetic modeling, using SRTM2 (41), was applied to generate a parametric BP_{ND} image for each animal. Subsequently, averaged BP_{ND} images were calculated for all groups. For visualization purposes, these images were smoothed using an isotropic Gaussian filter (full width at half maximum = 0.5 mm).

Data and Statistical Analysis

All statistical analysis was performed in GraphPad Prism 8 (GraphPad Software), and a significance level of $p < .05$ was imposed. The analysis of the behavioral data was performed according to a previously described protocol (34). To compare behavioral parameters between both genotypes, a Mann-Whitney *U* test was performed. All behavioral data are expressed as the averaged parameter-of-interest ± standard error for both the WT and the KO groups.

For both experiments 1 and 2, a Shapiro-Wilk test confirmed the normality for the VOI-based μPET data. A two-way analysis of variance with post hoc Bonferroni correction for multiple comparisons was applied to investigate whether significant regional differences were present between the test and blocking conditions (with repeated measures) and between the genotypes (without repeated measures). For experiment 2, comparing two genotypes, the analysis includes Cohen's *d* effect size. All imaging data are represented as the averaged value ± SD.

A voxel-based analysis was performed on the filtered BP_{ND} images using SPM12 (Wellcome Department of Imaging Neuroscience) in MATLAB (version R2016a; The MathWorks, Inc.). Statistical T-maps were calculated at a significance level of $p = .01$ and a cluster threshold of 100 voxels (voxel size: 0.09 × 0.09 × 0.09 mm).

The Pearson *r* correlation was used to determine the relationship between the outcome [^{11}C]ABP688 and [^{18}F]FPEB regional BP_{ND} values (cortex, striatum, hippocampus, and amygdala) of individual animals.

RESULTS

Significant Reductions in the BP_{ND} of High-Binding Brain Regions Upon Blocking of [^{11}C]ABP688 or [^{18}F]FPEB Supports Their Common Binding Site In Vivo

To directly verify the common binding site of ABP6888 and FPEB in vivo, a blocking study was performed (Figure S1—experiment 1). Based on the standard uptake value TACs (Figure 1), both tracers showed a rapid brain uptake within the first 10 minutes in different brain regions. Moreover, both blocking conditions using unlabeled ABP688 and unlabeled FPEB, resulted in a decrease of the standard uptake value TACs of high-binding brain regions toward the level of the cerebellar reference region. Correspondingly, both the [^{11}C]ABP688 BP_{ND} and the [^{18}F]FPEB BP_{ND} were significantly reduced in all investigated regions following the FPEB and the ABP688 pretreatment, respectively. Regional BP_{ND} estimates ±SD are reported in Table 1 (two-way repeated-measures analysis of variance: [^{11}C]ABP688 main effect of brain region $F_{3,24} = 2.906$, $p = .0554$; main effect of condition $F_{1,24} = 1209$, $p < .0001$; main effect of subject $F_{24} = 1.087$, $p = .4202$; main effect of brain region × condition $F_{3,24} = 3.424$, $p = .0332$—[^{18}F]FPEB main effect of brain region $F_{3,24} = 2.447$, $p = .0883$; main effect of condition $F_{1,24} = 863.1$, $p < .0001$; main effect of subject $F_{24} = 2.214$, $p = .0286$; main effect of brain region × condition $F_{3,24} = 11.86$, $p < .0001$).

The Presence of Compulsive-like Grooming Behavior Is Confirmed in the *Sapap3* KO Mice

In line with a previous and more extensive longitudinal characterization of compulsive-like grooming behavior in *Sapap3* KO mice (34), the grooming frequency (WT: 10.57 ± 1.53, KO: 46.50 ± 7.49, $p < .001$) and the % duration grooming (WT: 5.71 ± 1.24%, KO: 32.71 ± 7.50%, $p = .0046$) were significantly higher in the KO group, compared to WT control mice (Figure 2). Moreover, these values were of the same magnitude.

Both [^{11}C]ABP688 and [^{18}F]FPEB Measure Lower mGluR5 Availability in *Sapap3* KO Mice, but With Different Statistical Significance Compared With WT Control Mice

The resulting (A) BP_{ND} parametric images with the corresponding (B) VOI-based BP_{ND} values for both genotypes and radioligands are represented in Figure 3. For [^{11}C]ABP688, a cross-sectional comparison between genotypes revealed a significantly lower BP_{ND} in the cortex (−23.12%, $p = .0003$), striatum (−26.46%, $p < .0001$), hippocampus (−25.90%, $p < .0001$), and amygdala (−24.38%, $p = .0001$) of KO mice. On the other hand, for [^{18}F]FPEB, a more subtle BP_{ND} decline was significant for the striatum (−18.34%, $p = .0132$), hippocampus (−16.55%, $p = .0192$), and amygdala (−17.72%, $p = .0442$). All regional BP_{ND} estimates ± SD are reported in Table 2 (two-way analysis of variance: [^{11}C]ABP688 main effect of brain region $F_{3,60} = 11.03$, $p < .0001$; main effect of genotype $F_{1,60} = 101.2$, $p < .0001$; main effect of brain region × genotype $F_{3,60} = 0.6404$, $p = .5920$—[^{18}F]FPEB main effect of brain region $F_{3,60} = 21.70$, $p < .0001$; main effect of genotype $F_{1,60} = 27.59$, $p < .0001$; main effect of brain region x genotype $F_{3,60} = 0.2725$, $p = .8450$).

A more sensitive voxel-based analysis confirmed the established VOI-based significant differences in [^{11}C]ABP688 and [^{18}F]FPEB BP_{ND} between the genotypes. Figure 4 shows a significantly lower [^{11}C]ABP688 BP_{ND} in 80.37% of all voxels within the total striatal volume ($p < .001$; cluster threshold = 100) of the KO group. This significant BP_{ND} decrease was also present in a substantial part of the voxels from other regions (cortex: 40.00%, hippocampus: 54.75%, and amygdala: 50.38%). In comparison, the [^{18}F]FPEB BP_{ND} was significantly lower in 77.88% of all voxels within the striatal volume ($p < .01$; cluster

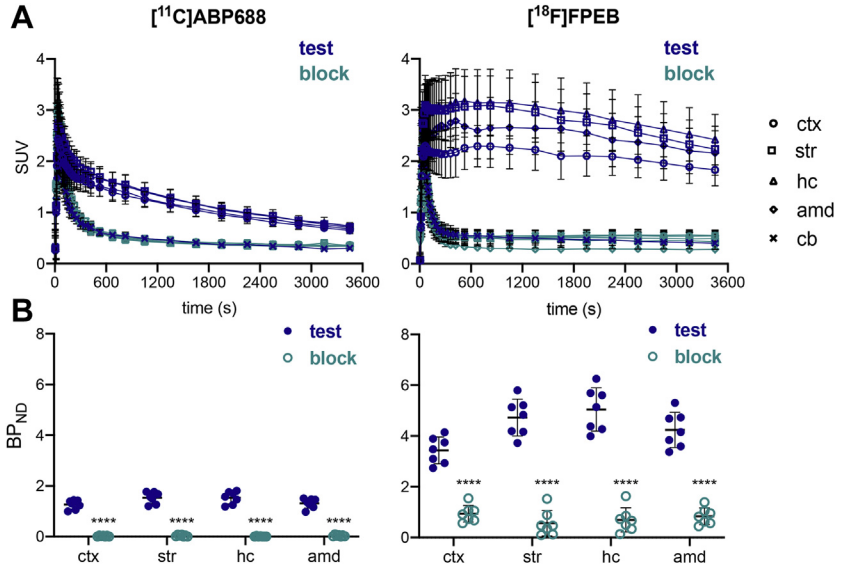

Figure 1. Target engagement of mGluR5 radioligands in the wild-type mouse brain. **(A)** Average regional [^{11}C]ABP688 and [^{18}F]FPEB time-activity curves (60-min acquisition) expressed in standardized uptake values with (block) and without (test) a pretreatment with cold FPEB or cold ABP688. All the time-activity curves of the high-binding regions decrease to the level of the cerebellar reference curve for both radioligands. **(B)** The corresponding BP_{ND} values for the blocking condition are significantly reduced in all investigated brain regions, when compared with the test condition (Table 1). ****$p < .0001$. amd, amygdala; BP_{ND}, nondisplaceable binding potential; cb, cerebellum; ctx, cortex; hc, hippocampus; str, striatum; SUV, standard uptake value.

Table 1. The Blocking Effect of Cold FPEB and Cold ABP688 on [^{11}C]ABP688 and [^{18}F]FPEB Binding, Respectively, via the Simplified Reference Tissue Model Quantification of the Regional BP_{ND} Values for a 60-Minute Dynamic Micro-PET Acquisition in WT Mice

	[^{11}C]ABP688 Test		[^{11}C]ABP688 Block		[^{18}F]FPEB Test		[^{18}F]FPEB Block	
Region	BP_{ND}, Mean ± SD	COV, %	BP_{ND}, Mean ± SD	Diff, −%	BP_{ND}, Mean ± SD	COV, %	BP_{ND}, Mean ± SD	Diff, −%
Ctx	1.26 ± 0.18	14.1%	0.02 ± 0.02	98.4%[a]	3.43 ± 0.53	15.3%	0.94 ± 0.33	72.7%[a]
Str	1.54 ± 0.23	14.9%	0.04 ± 0.01	97.6%[a]	4.72 ± 0.50	15.4%	0.56 ± 0.50	88.1%[a]
Hipp	1.54 ± 0.25	16.1%	0.01 ± 0.01	99.6%[a]	5.01 ± 0.85	16.9%	0.69 ± 0.48	86.2%[a]
Amy	1.31 ± 0.19	14.8%	0.04 ± 0.03	97.2%[a]	4.24 ± 0.70	16.4%	0.84 ± 0.33	80.3%[a]

Amy, amygdala; BP_{ND}, nondisplaceable binding potential; COV, coefficient of variation; Ctx, cortex; Diff, difference; Hipp, hippocampus; PET, positron emission tomography; Str, striatum; WT, wild-type.

[a]$p < .0001$.

threshold = 100). For the cortex, hippocampus, and amygdala, a significantly lower BP_{ND} in KO mice was found in 28.81%, 49.24%, and 47.72% of all voxels, respectively. Notably, when a stricter significance level of $p < .001$ was imposed on the [^{18}F]FPEB BP_{ND} data, similar to the level imposed on [^{11}C]ABP688 BP_{ND} data, the percentage of significant voxel declined to <0.6% for all the aforementioned regions.

The Intra-animal Relationship Between [^{11}C]ABP688 and [^{18}F]FPEB

A comparison between the [^{11}C]ABP688 and the [^{18}F]FPEB PET BP_{ND} values across all regions of interest (cortex, striatum, hippocampus, amygdala) per animal resulted in a strong correlation ($r = 0.8282$, $p < .0001$) for experiment 1 and a moderate correlation ($r = 0.5642$, $p < .001$) for experiment 2 including both WT and KO animals. When combining BP_{ND} values for the WT animals from both experiments, again a strong correlation (all regions: $r = 0.7187$, $p < .0001$; regional: cortex: $r = 0.5939$, $p = .0323$; striatum: $r = 0.6208$, $p = .0236$; hippocampus: $r = 0.6473$, $p = .0168$; amygdala: $r = 0.5023$, $p = .0803$) between the two mGluR5 radioligands could be demonstrated (Figure S2A). When only the KO animals from experiment 2 were considered, a similar comparison resulted in a moderate correlation (all regions: $r = 0.4042$, $p = .0097$; regional: cortex: $r = 0.0608$, $p = .8674$; striatum: $r = 0.2615$, $p = .4655$; hippocampus: $r = 0.1057$, $p = .7714$; amygdala: $r = 0.2480$, $p = .4987$) (Figure S2B).

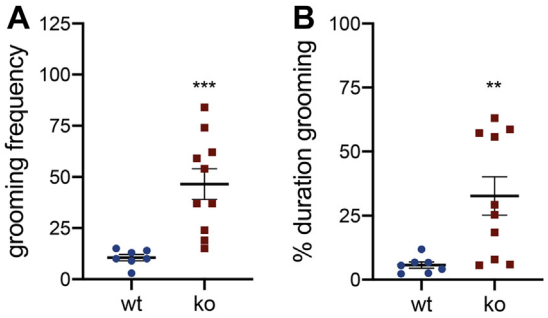

Figure 2. Validation of compulsive-like grooming in 9-month-old *Sapap3* knockout vs. wild-type control mice reflected by behavioral parameters: **(A)** grooming frequency and **(B)** % duration grooming. $^{**}p < .01$, $^{***}p < .001$. ko, knockout; wt, wild-type.

DISCUSSION

The study goals included the following: 1) setting up a blocking μPET paradigm to verify the common binding site for both [^{11}C]ABP688 and [^{18}F]FPEB at the mGluR5 allosteric site in vivo and in a direct manner; 2) providing a direct comparison between both radioligands in the robust *Sapap3* KO animal OCD model, which was earlier characterized by a lowered in vivo mGluR5 availability; and 3) generating direct intra-animal comparisons between mGluR5 availability measurements with both radioligands. Taken together, this setup allows a further investigation of the lower regional mGluR5 availability in the *Sapap3* KO mouse model exhibiting compulsive-like behavior (34). Through this preclinical step, we seek to contribute to future applications of mGluR5 radioligands in a clinical setting and to gather additional information on the role of mGluR5 in the pathophysiology of OCD and as a target for potential novel drug candidates.

In the blocking paradigm, we observed global reductions in mGluR5 availability (BP_{ND}) of approximately 98% for [^{11}C]ABP688 and 82% for [^{18}F]FPEB. It might appear that unlabeled ABP688 is only able to partially block [^{18}F]FPEB, suggesting the possibility of a second binding site. For this reason, the [^{18}F]FPEB blocking paradigm of experiment 1 was repeated in a satellite cohort of WT mice (Table S2) with a double dose of unlabeled ABP688 solution, and this in a 10% (instead of 5%) DMSO saline solution to further increase ABP688 solubility. With this adjusted setup, an average blocking percentage of 96% was achieved (Table S3; Figure S3). For all blocking experiments, the obtained regional high-binding TACs decreased to a similar level as the cerebellar reference curve, thereby further substantiating the specificity of both radioligands for their target. This supports the current body of literature (33,42,43), which already provided strong, but indirect, arguments for the same or close to the same binding site for both [^{11}C]ABP688 and [^{18}F]FPEB. First, previous preclinical PET studies showed blocking of the binding of these radioligands using other mGluR5 negative allosteric modulators (MPEP and MTEP) in different species for both [^{11}C]ABP688 [MPEP in rats (22,32), MPEP in mice (27), and MTEP in baboons (31)] and [^{18}F]FPEB [MTEP in rats (23,26) and rhesus monkeys (44)]. Moreover, clinical studies have already explored whether [^{18}F]FPEB was able to reproduce [^{11}C]ABP688 results obtained in healthy control mice. DeLorenzo *et al.* (33) provided an indirect comparison between same-day test-retest [^{11}C]ABP688 and [^{18}F]FPEB PET

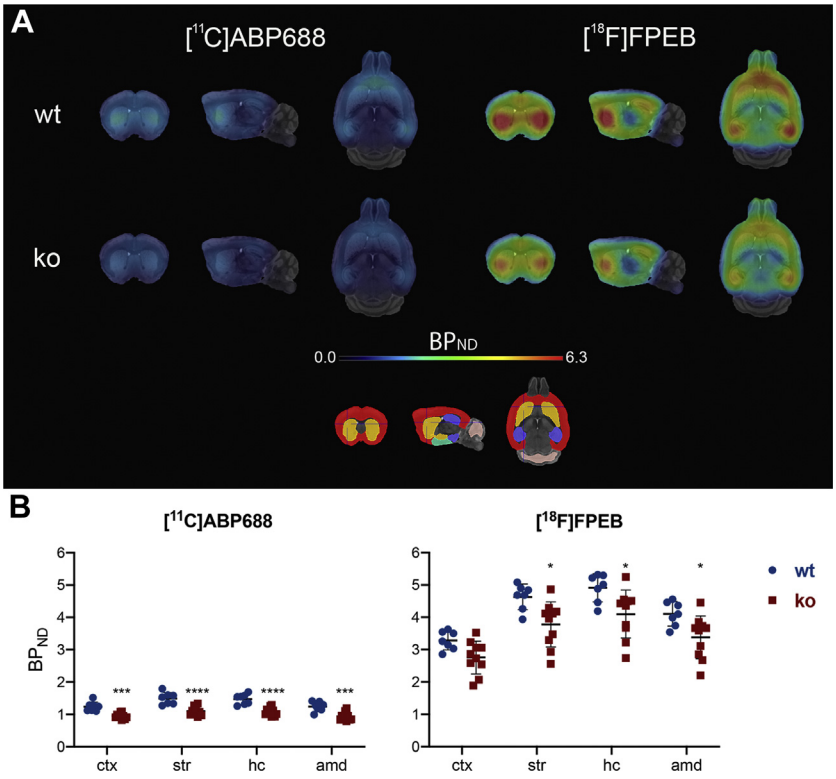

Figure 3. Micro-PET imaging of mGluR5 radioligands in the wild-type vs. the *Sapap3* knockout mouse brain. **(A)** Average [^{11}C]ABP688 and [^{18}F]FPEB micro-PET BP_{ND} (simplified reference tissue model 2) parametric images superimposed on a mouse template (red: ctx; yellow: str; purple: hc; green: amd; pink: cb reference region) **(B)** combined with the corresponding averaged [^{11}C]ABP688 and [^{18}F]FPEB PET BP_{ND} values ± SD (Table 2). *$p < .05$, ***$p < .001$, ****$p < .0001$. amd, amygdala; BP_{ND}, nondisplaceable binding potential; cb, cerebellum; ctx, cortex; hc, hippocampus; ko, knockout; PET, positron emission tomography; str, striatum; wt, wild-type.

measurements in healthy subjects. They show a significantly higher estimated BP_{ND}' for both [^{11}C]ABP688 and [^{18}F]FPEB in the retest scan, indicating consistency between the findings for both radioligands.

Second, both radioligands were directly compared in the *Sapap3* KO mice, previously shown to possess a decreased mGluR5 availability for [^{11}C]ABP688 (34) parallel to the worsening of OCD-like grooming behavior (16). Possibly, this reduced mGluR5 availability within the cortico-striato-thalamocortical OCD circuitry is associated with excessive mGluR5 signaling in this model via constitutive activation mechanisms (16,45). As the BP_{ND} parameter is proportional to the affinity and the availability (and possibly expression) of the receptor (46), changes in these parameters, such as receptor internalization (47), could also explain the decreased binding of both radioligands in *Sapap3* KO mice. Future studies should seek to clarify the mechanisms underlying such alterations in mGluR5 availability. As anticipated, [^{18}F]FPEB was also able to pick up group differences between KO mice and WT control mice but to a lesser extent. The significance levels were lower and limited to a smaller number of regions when compared with [^{11}C]ABP688. Moreover, parallels exist with previous clinical findings, despite species differences. A study in healthy control mice showed that the [^{11}C]ABP688 regional V_T decreased on average by 21.3 ± 21.4% on infusion with a subanesthetic dose of ketamine, when compared with a baseline scan on the same day (48). A second study, with a similar setup combining [^{11}C]ABP688 PET with a ketamine

Table 2. Overview of the Average [^{11}C]ABP688 and [^{18}F]FPEB Micro-PET BP_{ND} Values of WT Versus *Sapap3* KO Mice

	[^{11}C]ABP6888 WT		[^{11}C]ABP688 KO				[^{18}F]FPEB WT		[^{18}F]FPEB KO			
Region	BP_{ND}, Mean ± SD	COV, %	BP_{ND}, Mean ± SD	COV, %	Diff, −%	Eff. *d*	BP_{ND}, Mean ± SD	COV, %	BP_{ND}, Mean ± SD	COV, %	Diff, −%	Eff. *d*
Ctx	1.24 ± 0.14	11.7%	0.95 ± 0.09	9.2%	23.1%[a]	2.46	3.28 ± 0.29	8.8%	2.76 ± 0.51	18.4%	16.0%	1.25
Str	1.49 ± 0.18	12.4%	1.10 ± 0.14	12.3%	26.5%[b]	2.42	4.63 ± 0.40	8.6%	3.78 ± 0.70	18.5%	18.3%[c]	1.49
Hipp	1.47 ± 0.16	11.0%	1.09 ± 0.13	11.5%	25.9%[b]	2.92	4.91 ± 0.44	8.9%	4.10 ± 0.74	18.1%	16.6%[c]	1.33
Amy	1.24 ± 0.15	13.4%	0.94 ± 0.13	13.5%	24.4%[a]	2.14	4.11 ± 0.38	9.2%	3.38 ± 0.66	19.6%	17.7%[c]	1.36

Amy, amygdala; BP_{ND}, nondisplaceable binding potential; COV, coefficient of variation; Ctx, cortex; Diff, difference; Eff. *d*, effect size Cohen's *d*; Hipp, hippocampus; KO, knockout; PET, positron emission tomography; Str, striatum; WT, wild-type.

[a]$p < .001$.

[b]$p < .0001$.

[c]$p < .05$.

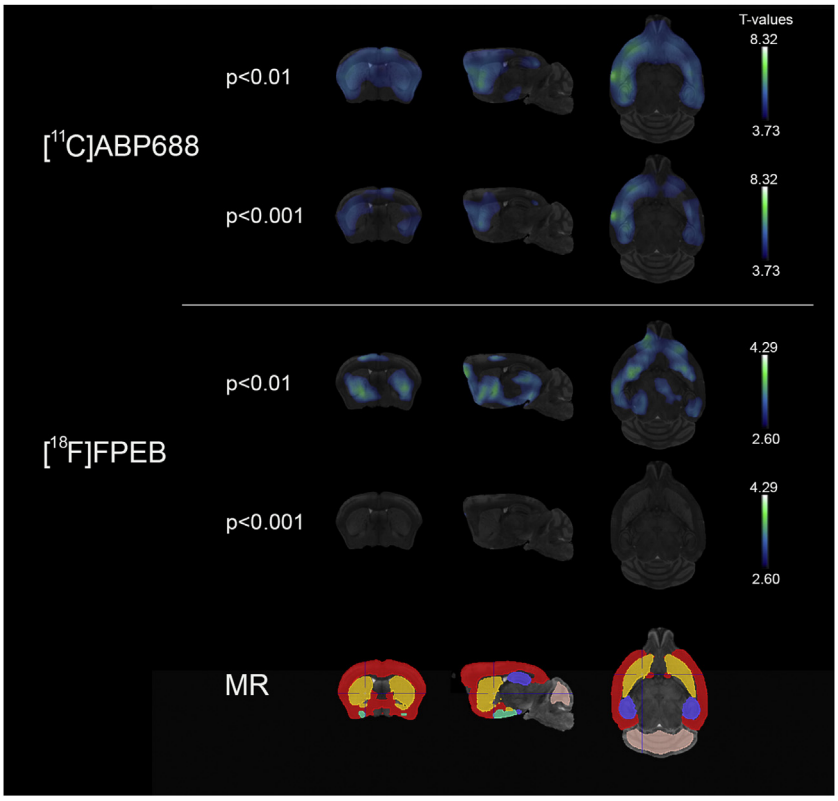

Figure 4. Voxel-based analysis via statistical parametric mapping of micro-PET imaging of mGluR5 radioligands in the WT vs. the *Sapap3* KO mouse brain. Hypo T-maps (voxel-based analysis) superimposed on a mouse template (red: ctx; yellow: str; purple: hc; green: amd; pink: cb reference region) showing clusters of voxels (threshold = 100 voxels) with a significantly lower BP_{ND} in the KO group vs. the WT group for [^{11}C]ABP688 ($p < .01$) and [^{18}F]FPEB ($p < .001$), respectively. amd, amygdala; BP_{ND}, nondisplaceable binding potential; ctx, cortex; hc, hippocampus; KO, knockout; MR, magnetic resonance; PET, positron emission tomography; str, striatum; WT, wild-type.

challenge in patients with major depressive disorder and healthy control subjects (49), also reported a significant ketamine-induced decrease in [^{11}C]ABP688 binding of the same magnitude as the previous study for healthy control subjects (−19 ± 22%). Patients with major depressive disorder, who already had significantly lower baseline binding levels, also showed a significant decrease in binding with the ketamine challenge (−14 ± 9%). In a third [^{18}F]FPEB study, again with a similar setup, the ketamine-induced changes in mGluR5 availability were of smaller magnitude (circa 10%) (42). These findings suggest the possible superiority of [^{11}C]ABP688 in detecting mGluR5 changes in drug challenge paradigms. The current findings in *Sapap3* KO mice characterized by intrinsic mGluR5 abnormalities further support these findings: [^{11}C]ABP688 BP_{ND} decreased on average with circa 25%, and [^{18}F]FPEB BP_{ND} decreased on average with 17% compared with WT control mice. Also, in the current study the limitations of possible dynamic effects of a glutamate modulating compound, such as ketamine, on tracer delivery and washout were circumvented. The combination of the current findings suggests that [^{11}C]ABP688 is more suitable to pick up mGluR5 differences in subjects with intrinsic mGluR5 abnormalities. Still, extrapolation of results to other models/species should be done with caution, keeping in mind the presence of (non)physiological sources of variability and the possible existence of the aforementioned diverse mechanisms underlying changes in mGluR5 availability. In addition, methodological and technical differences between studies could hamper the generalization of findings. For example for [^{18}F]FPEB, tracer dose conditions were assumed based on the absence of a negative correlation between the injected cold mass and the obtained BP_{ND} per animal. However, this has not yet been more rigorously demonstrated based on a wider range of unlabeled FPEB doses (50).

Multiple studies have shown that the timing of two consecutive PET scans for mGluR5 availability evaluation should be considered. Here, the test scans were separated by 4 or more days (experiment 1: 4.0 ± 0.0 days; experiment 2: WT 9.0 ± 2.8 days, KO 9.2 ± 2.3 days). Both human test-retest studies using either [^{11}C]ABP688 (51–53) or [^{18}F]FPEB (54,55) and rodent studies (26,27,50,56), with days to weeks between consecutive scans, reported sufficient test-retest stability. Based on these findings, we assume a low variability in mGluR5 availability within one subject between consecutive PET scans.

Third, this study design allowed a first within-subject, and consequently direct, comparison between the regional BP_{ND} values for both studied radioligands to verify possible radioligand superiority. In an unperturbed glutamate system, only considering the WT control mice, we found a strong correlation between the [^{11}C]ABP688 and the [^{18}F]FPEB regional BP_{ND} values. These findings again suggest that a similar pool of mGluR5 receptors is targeted by both ligands. In addition, when only considering subjects with a perturbed and especially lower mGluR5 availability (*Sapap3* KO mice), the correlation loses its strength.

In conclusion, this study provides a first direct comparison between [^{11}C]ABP688 and [^{18}F]FPEB, which will continue to

play a significant role in the understanding of disease mechanisms underlying psychiatric and neurologic disorders and their treatment. This study directly implies a competition between both radioligands for a common binding site at the level of the allosteric pocket of the receptor. Furthermore, both [^{11}C]ABP688 and [^{18}F]FPEB were able to quantify a lower brain mGluR5 availability in *Sapap3* KO mice showing OCD-like behavior. Considering individual WT mice, our results suggest a strong relationship between the BP_{ND} parameter for mGluR5 availability for both radioligands. Notwithstanding, compared with [^{18}F]FPEB, our data suggest that [^{11}C]ABP688 may be a more sensitive radiotracer for measuring mGluR5 availability in (models of) disease with intrinsic mGluR5 abnormalities such as the *Sapap3* KO mouse model. In summary, the current finding of a higher variability in regional BP_{ND} for [^{18}F]FPEB compared with [^{11}C]ABP688 in the brain of *Sapap3* KO mice suggests the use of [^{11}C]ABP688 when designing a PET study for mGluR5 quantification.

ACKNOWLEDGMENTS AND DISCLOSURES

This work was funded by Antwerp University, Belgium, through a Ph.D. grant for DG, a full professor position for SSta and SStr, and an assistant professor position for JV. Hardware and experimental costs were supported by a DOCPRO (41/FA020000/FFB140317) of the University of Antwerp and a Fonds Wetenschappelijk Onderzoek FWO KAN (42/FA020000/685).

No funding sources had a role in the study design or in the collection, analysis, and interpretation of the data; in the writing of the report; or in the decision to submit the paper for publication.

DG and SSta designed the study and wrote the protocol. DG managed the literature searches and analyses. SDL supervised the radiotracer productions. DG, JV, and AM performed image processing and statistical analysis, and DG wrote the first draft of the manuscript. SSta and SStr proofread the manuscript. All authors contributed to and have approved the final manuscript.

The authors report no biomedical financial interests or potential conflicts of interest.

ARTICLE INFORMATION

From the Molecular Imaging Center Antwerp (DG, JV, AM, SDL, SStr, SSta), University of Antwerp, Wilrijk; and the Department of Nuclear Medicine (SDL, SStr), Antwerp University Hospital, Edegem, Belgium.

Address correspondence to Steven Staelens, Ph.D., at steven.staelens@uantwerpen.be.

Received Jun 25, 2021; revised Nov 17, 2021; accepted Nov 20, 2021.

Supplementary material cited in this article is available online at https://doi.org/10.1016/j.bpsc.2021.11.010.

REFERENCES

1. Esterlis I, Holmes SE, Sharma P, Krystal JH, DeLorenzo C (2018): Metabotropic glutamatergic receptor 5 and stress disorders: Knowledge gained from receptor imaging studies. Biol Psychiatry 84:95–105.
2. Pillai RLI, Tipre DN (2016): Metabotropic glutamate receptor 5—A promising target in drug development and neuroimaging. Eur J Nucl Med Mol Imaging 43:1151–1170.
3. Ruscio AM, Stein DJ, Chiu WT, Kessler RC (2010): The epidemiology of obsessive-compulsive disorder in the National Comorbidity Survey Replication. Mol Psychiatry 15:53–63.
4. Abramowitz JS, Taylor S, McKay D (2009): Obsessive-compulsive disorder. Lancet 374:491–499.
5. American Psychiatric Association (2013): Diagnostic and Statistical Manual of Mental Disorders, 5th ed. Arlington: American Psychiatric Association.
6. Denys D, Mantione M, Figee M, Van Den Munckhof P, Koerselman F, Westenberg H, *et al.* (2010): Deep brain stimulation of the nucleus accumbens for treatment-refractory obsessive-compulsive disorder. Arch Gen Psychiatry 67:1061–1068.
7. Pittenger C, Bloch MH, Williams K (2011): Glutamate abnormalities in obsessive compulsive disorder: Neurobiology, pathophysiology, and treatment. Pharmacol Ther 132:314–332.
8. Wu K, Hanna GL, Rosenberg DR, Arnold PD (2012): The role of glutamate signaling in the pathogenesis and treatment of obsessive-compulsive disorder. Pharmacol Biochem Behav 100:726–735.
9. International Obsessive Compulsive Disorder Foundation Genetics Collaborative (IOCDF-GC) and OCD Collaborative Genetics Association Studies (OCGAS) (2018): Revealing the complex genetic architecture of obsessive-compulsive disorder using meta-analysis. Mol Psychiatry 23:1181–1188.
10. Aida T, Yoshida J, Nomura M, Tanimura A, Iino Y, Soma M, *et al.* (2015): Astroglial glutamate transporter deficiency increases synaptic excitability and leads to pathological repetitive behaviors in mice. Neuropsychopharmacology 40:1569–1579.
11. Jia YF, Wininger K, Ho AMC, Peyton L, Baker M, Choi DS (2020): Astrocytic glutamate Transporter 1 (GLT1) deficiency reduces anxiety- and depression-like behaviors in mice. Front Behav Neurosci 14:57.
12. Welch JM, Lu J, Rodriguiz RM, Trotta NC, Peca J, Ding JD, *et al.* (2007): Cortico-striatal synaptic defects and OCD-like behaviours in Sapap3-mutant mice. Nature 448:894–900.
13. Zhang XY, Peng SY, Shen LP, Zhuang QX, Li B, Xie ST, *et al.* (2020): Targeting presynaptic H3 heteroreceptor in nucleus accumbens to improve anxiety and obsessive-compulsive-like behaviors. Proc Natl Acad Sci U S A 117:32155–32164.
14. Delgado-Acevedo C, Estay SF, Radke AK, Sengupta A, Escobar AP, Henríquez-Belmar F, *et al.* (2019): Behavioral and synaptic alterations relevant to obsessive-compulsive disorder in mice with increased EAAT3 expression. Neuropsychopharmacology 44:1163–1173.
15. Niswender CM, Conn PJ (2010): Metabotropic glutamate receptors: Physiology, pharmacology, and disease. Annu Rev Pharmacol Toxicol 50:295–322.
16. Ade KK, Wan Y, Hamann HC, O'Hare JK, Guo W, Quian A, *et al.* (2016): Increased metabotropic glutamate receptor 5 signaling underlies obsessive-compulsive disorder-like behavioral and striatal circuit abnormalities in mice. Biol Psychiatry 80:522–533.
17. Goodman WK, Storch EA, Sheth SA (2021): Harmonizing the neurobiology and treatment of obsessive-compulsive disorder. Am J Psychiatry 178:17–29.
18. Grassi G, Cecchelli C, Vignozzi L, Pacini S (2020): Investigational and experimental drugs to treat obsessive-compulsive disorder. J Exp Pharmacol 12:695–706.
19. Rutrick D, Stein DJ, Subramanian G, Smith B, Fava M, Hasler G, *et al.* (2017): Mavoglurant augmentation in OCD patients resistant to selective serotonin reuptake inhibitors: A proof-of-concept, randomized, placebo-controlled, phase 2 study. Adv Ther 34:524–541.
20. Grassi G, Pallanti S (2018): Current and up-and-coming pharmacotherapy for obsessive-compulsive disorder in adults. Expert Opin Pharmacother 19:1541–1550.
21. Kim JH, Marton J, Ametamey SM, Cumming P (2020): A review of molecular imaging of glutamate receptors. Molecules 25:4749.
22. Ametamey SM, Kessler LJ, Honer M, Wyss MT, Buck A, Hintermann S, *et al.* (2006): Radiosynthesis and preclinical evaluation of 11C-ABP688 as a probe for imaging the metabotropic glutamate receptor subtype 5. J Nucl Med 47:698–705.
23. Wang JQ, Tueckmantel W, Zhu A, Pellegrino D, Brownell AL (2007): Synthesis and preliminary biological evaluation of 3-[(18)F]fluoro-5-(2-pyridinylethynyl)benzonitrile as a PET radiotracer for imaging metabotropic glutamate receptor subtype 5. Synapse 61:951–961.
24. Dupont AC, Serrière S, Barantin L, Vercouillie J, Tauber C, Gissot V, *et al.* (2021): Study of influence of the glutamatergic concentration of [18F]FPEB binding to metabotropic glutamate receptor subtype 5 with

N-acetylcysteine challenge in rats and SRM/PET study in human healthy volunteers. Transl Psychiatry 11:66.
25. Lin X, Donthamsetti P, Skinberg M, Slifstein M, Abi-Dargham A, Javitch J (2015): FPEB and ABP688 Cannot Accesss Internalized MGluR5 Receptors. mGluR5 Workshop. Yale University.
26. De Laat B, Leurquin-Sterk G, Celen S, Bormans G, Koole M, Van Laere K, Casteels C (2015): Preclinical evaluation and quantification of 18F-FPEB as a radioligand for PET imaging of the metabotropic glutamate receptor 5. J Nucl Med 56:1954–1959.
27. Verhaeghe J, Bertoglio D, Kosten L, Thomae D, Verhoye M, Van Der Linden A, *et al.* (2018): Noninvasive relative quantification of [11C] ABP688 PET imaging in mice versus an input function measured over an arteriovenous shunt. Front Neurol 9:516.
28. Patel S, Hamill TG, Connolly B, Jagoda E, Li W, Gibson RE (2007): Species differences in mGluR5 binding sites in mammalian central nervous system determined using in vitro binding with [18F]F-PEB. Nucl Med Biol 34:1009–1017.
29. Akkus F, Terbeck S, Ametamey SM, Rufer M, Treyer V, Burger C, *et al.* (2014): Metabotropic glutamate receptor 5 binding in patients with obsessive-compulsive disorder. Int J Neuropsychopharmacol 17:1915–1922.
30. Rook JM, Tantawy MN, Ansari MS, Felts AS, Stauffer SR, Emmitte KA, *et al.* (2015): Relationship between in vivo receptor occupancy and efficacy of metabotropic glutamate receptor subtype 5 allosteric modulators with different in vitro binding profiles. Neuropsychopharmacology 40:755–765.
31. Delorenzo C, Milak MS, Brennan KG, Kumar JSD, Mann JJ, Parsey RV (2011): In vivo positron emission tomography imaging with [^{11}C] ABP688: Binding variability and specificity for the metabotropic glutamate receptor subtype 5 in baboons. Eur J Nucl Med Mol Imaging 38:1083–1094.
32. Elmenhorst D, Minuzzi L, Aliaga A, Rowley J, Massarweh G, Diksic M, *et al.* (2010): In vivo and in vitro validation of reference tissue models for the mGluR (5) ligand [11C]ABP688. J Cereb Blood Flow Metab 30:1538–1549.
33. DeLorenzo C, Gallezot JD, Gardus J, Yang J, Planeta B, Nabulsi N, *et al.* (2017): In vivo variation in same-day estimates of metabotropic glutamate receptor subtype 5 binding using [11C]ABP688 and [18F] FPEB. J Cereb Blood Flow Metab 37:2716–2727.
34. Glorie D, Verhaeghe J, Miranda A, Kertesz I, Wyffels L, Stroobants S, Staelens S (2020): Progression of obsessive compulsive disorder-like grooming in Sapap3 knockout mice: A longitudinal [11C]ABP688 PET study. Neuropharmacology 177:108160.
35. O'Connor EC, Bariselli S, Bellone C (2014): Synaptic basis of social dysfunction: A focus on postsynaptic proteins linking group-I mGluRs with AMPARs and NMDARs. Eur J Neurosci 39:1114–1129.
36. Welch JM, Wang D, Feng G (2004): Differential mRNA expression and protein localization of the SAP90/PSD-95-associated proteins (SAPAPs) in the nervous system of the mouse. J Comp Neurol 472: 24–39.
37. Hume SP, Gunn RN, Jones T (1998): Pharmacological constraints associated with positron emission tomographic scanning of small laboratory animals. Eur J Nucl Med 25:173–176.
38. Miranda A, Bertoglio D, Glorie D, Stroobants S, Staelens S, Verhaeghe J (2020): Validation of a spatially variant resolution model for small animal brain PET studies. Biomed Phys Eng Express 6:045001.
39. Johnson GA, Badea A, Brandenburg J, Cofer G, Fubara B, Liu S, Nissanov J (2010): Waxholm Space: An image-based reference for coordinating mouse brain research. Neuroimage 53:365–372.
40. Lammertsma AA, Hume SP (1996): Simplified reference tissue model for PET receptor studies. Neuroimage 4:153–158.
41. Wu Y, Carson RE (2002): Noise reduction in the simplified reference tissue model for neuroreceptor functional imaging. J Cereb Blood Flow Metab 22:1440–1452.
42. Holmes SE, Gallezot JD, Davis MT, DellaGioia N, Matuskey D, Nabulsi N, *et al.* (2020): Measuring the effects of ketamine on mGluR5 using [18F]FPEB and PET. J Cereb Blood Flow Metab 40:2254–2264.
43. Kuwabara H, Chamroonrat W, Mathews W, Waterhouse R, Brasic J, Guevara MR, *et al.* (2011): Evaluation of 11C-ABP688 and 18F-FPEB for imaging mGluR5 receptors in the human brain. J Nucl Med 52:390.
44. Hamill TG, Krause S, Ryan C, Bonnefous C, Govek S, Seiders TJ, *et al.* (2005): Synthesis, characterization, and first successful monkey imaging studies of metabotropic glutamate receptor subtype 5 (mGluR5) PET radiotracers. Synapse 56:205–216.
45. Ango F, Prézeau L, Muller T, Tu JC, Xiao B, Worley PF, *et al.* (2001): Agonist-independent activation of metabotropic glutamate receptors by the intracellular protein Homer. Nature 411:962–965.
46. Innis RB, Cunningham VJ, Delforge J, Fujita M, Gjedde A, Gunn RN, *et al.* (2007): Consensus nomenclature for in vivo imaging of reversibly binding radioligands. J Cereb Blood Flow Metab 27:1533–1539.
47. Trivedi RR, Bhattacharyya S (2012): Constitutive internalization and recycling of metabotropic glutamate receptor 5 (mGluR5). Biochem Biophys Res Commun 427:185–190.
48. Delorenzo C, Dellagioia N, Bloch M, Sanacora G, Nabulsi N, Abdallah C, *et al.* (2015): In vivo ketamine-induced changes in [^{11}C] ABP688 binding to metabotropic glutamate receptor subtype 5. Biol Psychiatry 77:266–275.
49. Esterlis I, DellaGioia N, Pietrzak RH, Matuskey D, Nabulsi N, Abdallah CG, *et al.* (2018): Ketamine-induced reduction in mGluR5 availability is associated with an antidepressant response: An [11C] ABP688 and PET imaging study in depression. Mol Psychiatry 23:824–832.
50. Wyckhuys T, Verhaeghe J, Wyffels L, Langlois X, Schmidt M, Stroobants S, Staelens S (2013): N-acetylcysteine-and MK-801-induced changes in glutamate levels do not affect in vivo binding of metabotropic glutamate 5 receptor radioligand 11C-ABP688 in rat brain. J Nucl Med 54:1954–1961.
51. Burger C, Deschwanden A, Ametamey S, Johayem A, Mancosu B, Wyss M, *et al.* (2010): Evaluation of a bolus/infusion protocol for 11C-ABP688, a PET tracer for mGluR5. Nucl Med Biol 37:845–851.
52. Park E, Sullivan JM, Planeta B, Gallezot JD, Lim K, Lin SF, *et al.* (2015): Test–retest reproducibility of the metabotropic glutamate receptor 5 ligand [^{18}F]FPEB with bolus plus constant infusion in humans. Eur J Nucl Med Mol Imaging 42:1530–1541.
53. Smart K, Cox SML, Nagano-Saito A, Rosa-Neto P, Leyton M, Benkelfat C (2018): Test–retest variability of [^{11}C]ABP688 estimates of metabotropic glutamate receptor subtype 5 availability in humans. Synapse 72:e22041.
54. Wong DF, Waterhouse R, Kuwabara H, Kim J, Brašíc JR, Chamroonrat W, *et al.* (2013): 18F-FPEB, a PET radiopharmaceutical for quantifying metabotropic glutamate 5 receptors: A first-in-human study of radiochemical safety, biokinetics, and radiation dosimetry. J Nucl Med 54:388–396.
55. Leurquin-Sterk G, Postnov A, de Laat B, Casteels C, Celen S, Crunelle CL, *et al.* (2016): Kinetic modeling and long-term test-retest reproducibility of the mGluR5 PET tracer 18F-FPEB in human brain. Synapse 70:153–162.
56. Elmenhorst D, Aliaga A, Bauer A, Rosa-Neto P (2012): Test-retest stability of cerebral mGluR 5 quantification using [11C]ABP688 and positron emission tomography in rats. Synapse 66:552–560.